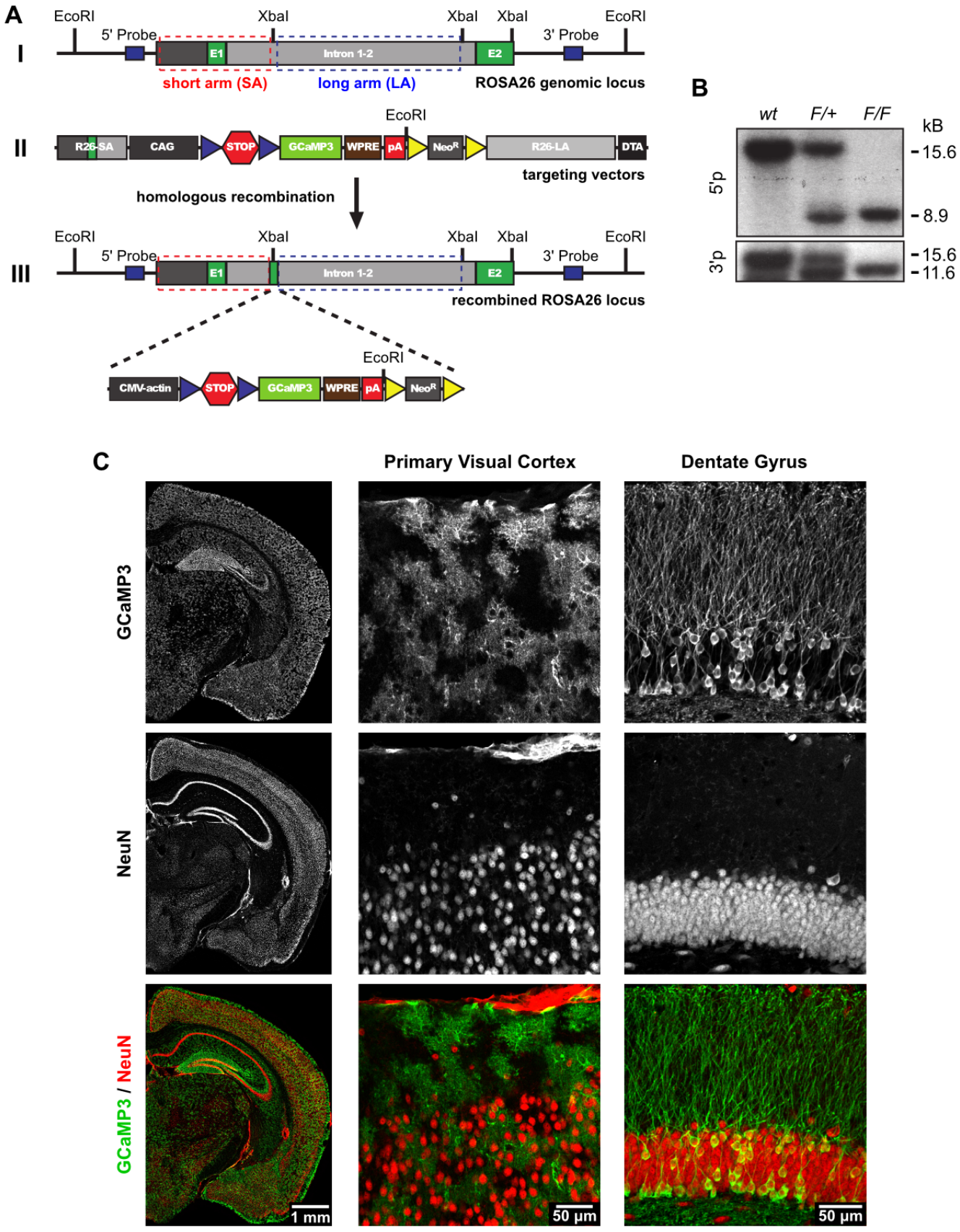
A
EcoRI
XbaI
XbaI
XbaI
EcoRI
5' Probe
3' Probe
I
E1
Intron 1-2
E2
short arm (SA)
long arm (LA)
ROSA26 genomic locus
EcoRI
II
R26-SA
CAG
STOP
GCaMP3
WPRE
pA
NeoR
R26-LA
DTA
targeting vectors
homologous recombination
EcoRI
XbaI
XbaI
XbaI
EcoRI
5' Probe
3' Probe
III
E1
Intron 1-2
E2
recombined ROSA26 locus
EcoRI
CMV-actin
STOP
GCaMP3
WPRE
pA
NeoR
B
wt
F/+
F/F
kB
5'p
15.6
8.9
3'p
15.6
11.6
C
Primary Visual Cortex
Dentate Gyrus
GCaMP3
NeuN
GCaMP3 / NeuN
1 mm
50 µm
50 µm

Figure S1

Figure S1 | Generation of conditional GCaMP3 transgenic mice, related to Figure 1. **A**, A gene trap strategy to 'knock in' GCaMP3 into the murine ROSA26 gene. (I) Genomic structure of the wildtype ROSA26 allele. The locus comprises two exons (E1 and E2; green boxes). The first XbaI restriction site located in intron 1-2 was used for gene trapping, mediated by homologous recombination in murine embryonic stem (ES) cells. (II) Structure of the GCaMP3 targeting vector. The construct harbors 5' (R26-SA) and 3' (R26-LA) homology arms from ROSA26, the CMV enhancer chicken β-actin hybrid (CAG) promoter (black box), loxP flanked 3x SV40-polyA "STOPPER" sequence (blue triangles and red hexagon), the GCaMP3 cDNA (light green box), Woodchuck post-transcriptional response element (WPRE, brown box), bovine growth hormone polyA sequence (pA, red box) and a neomycin resistance cassette (NeoR, black box) flanked by two FRT sites (yellow triangles). (III) ROSA26 allele after homologous recombination in murine ES cells. **B**, Southern blot analysis of genomic DNA extracted from mouse tail biopsies using 5' probe and 3' probes (indicated in Blue, in A I). The 5' probe detected one gene fragment of 15.6 kb in wildtype (wt), two fragments of 15.6 kb and 8.9 kb in heterozygous (F/+, R26-lsl-GCaMP3/wt) and one smaller fragment of 8.9 kb in homozygous mice (F/F, R26-lsl-GCaMP3/R26-lsl-GCaMP3). Similarly, the 3' probe detected one gene fragment of 15.6 kb in wildtype, two fragments of 15.6 kb and 11.6 kb in heterozygous, and one smaller fragment of 11.6 kb in homozygous mice. **C**, Coronal brain sections from a P28 GLAST-CreER;R26-lsl-GCaMP3 mouse that was injected with 2 mg (i.p.) 4-OH-tamoxifen at P14 (P14 + 14). (Left panels) Low magnification images of brain hemisections immunostained for GFP (GCaMP3) and NeuN (neurons) demonstrating widespread expression of GCaMP3. (Middle panels) Images of primary visual cortex (V1) showing $GCaMP3^+$ astrocytes in V1 that were $NeuN^-$. (Right panels)Images of $GCaMP3^+$ $NeuN^+$ granule neurons in the dentate gyrus. Images in the left panels were acquired using an epifluorescence microscope, and images in the middle and right panels were acquired using a laser scanning confocal microscope.

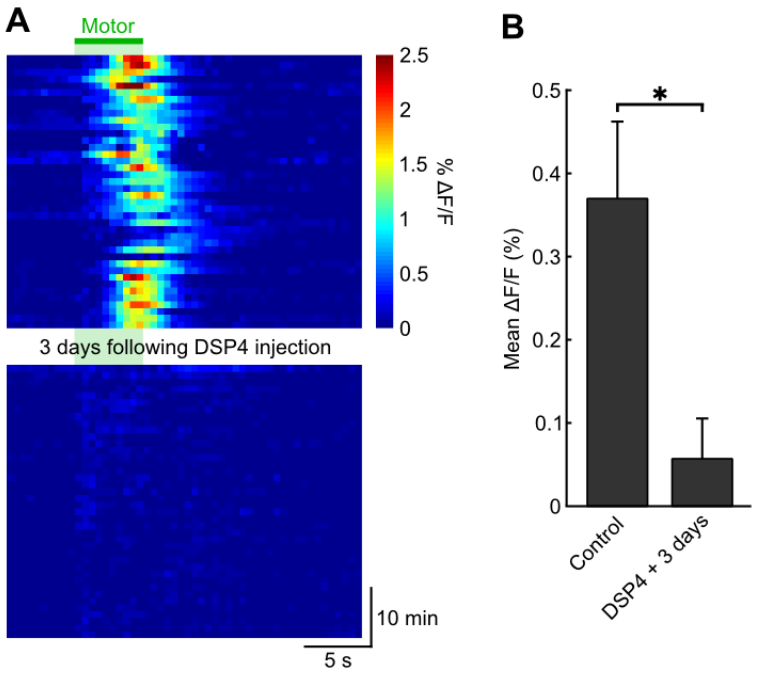

Figure S2 | Chemical disruption of noradrenergic signaling strongly reduces locomotion induced Ca^{2+} elevations in Bergmann glia, related to Figure 2. **A**, Pseudocolored plot of Ca^{2+} elevations (GCaMP3 fluorescence) in Bergmann glia in consecutive trials of enforced locomotion before (top panel) and three days following injection of DSP4 (50 mg/kg i.p.) (lower panel). Green bar highlights period of enforced locomotion. **B**, Summary of population data, bars and symbols represent mean ± SEM (n = 4 mice). Asterisk indicates significant reduction (one-tailed paired t test, p = 0.028).

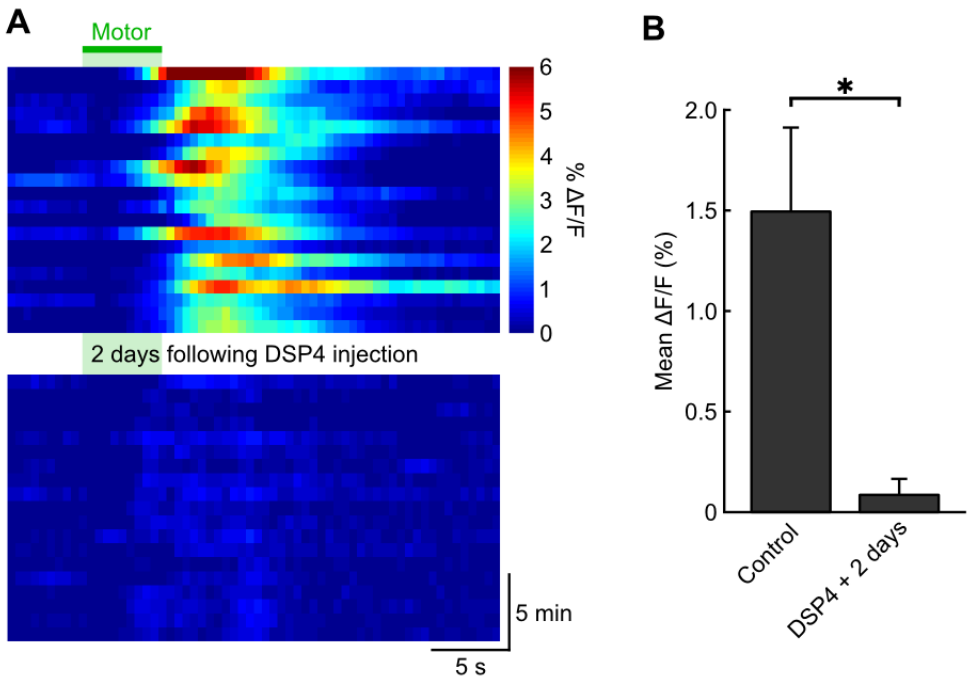

Figure S3 | Chemical disruption of noradrenergic signaling strongly reduces locomotion induced astrocyte Ca^{2+} elevations in primary visual cortex (V1), related to Figure 3. **A**, Pseudocolored plot of Ca^{2+} elevations in V1 astrocytes in consecutive trials of enforced locomotion before (top panel) and two days following injection of DSP4 (50 mg/kg i.p.) (lower panel). Green bar highlights period of enforced locomotion. **B**, Summary of population data, bars and symbols represent mean ± SEM (n = 4 mice). Asterisk indicates significant reduction (one-tailed paired t test, p = 0.030).

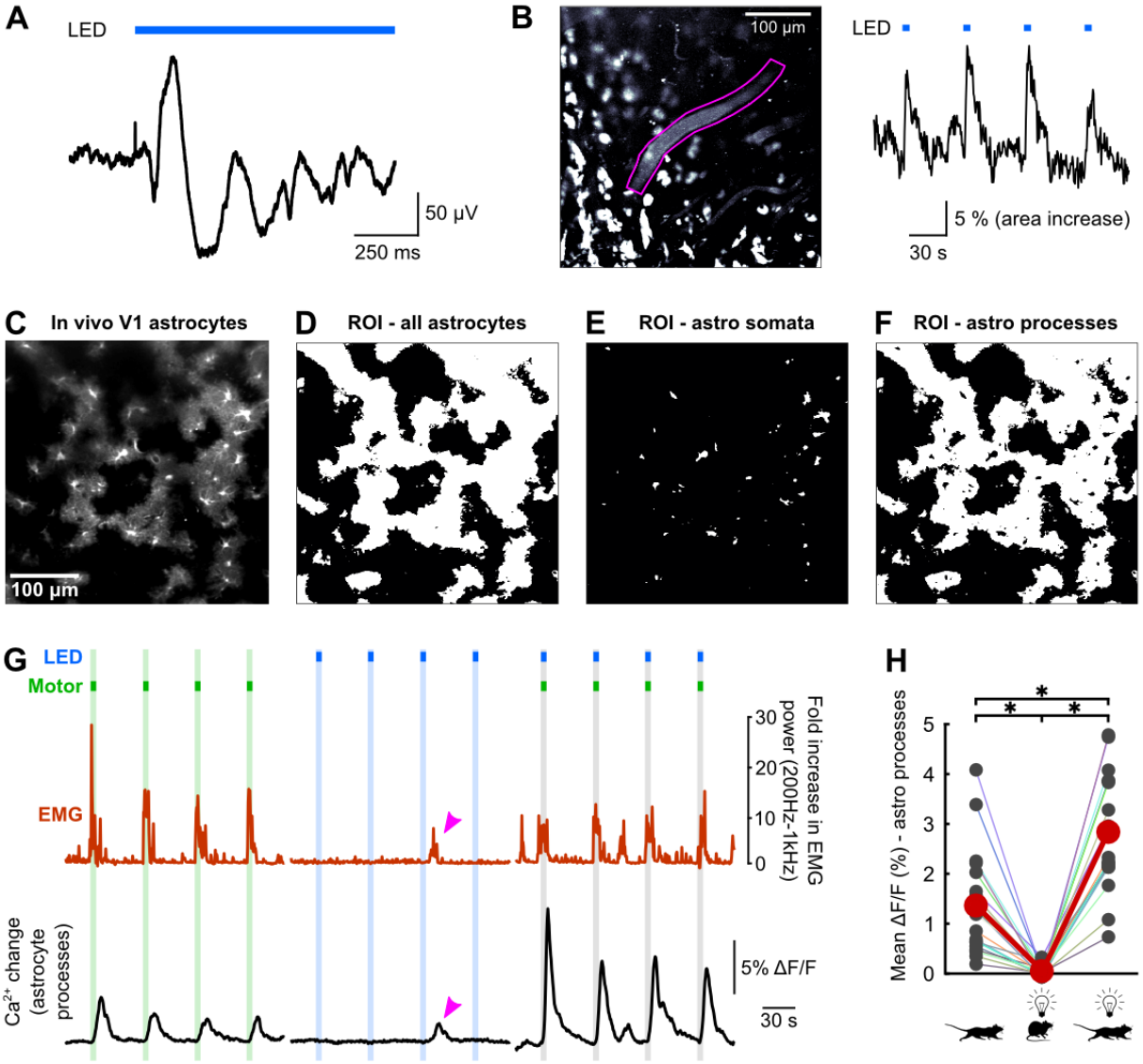

Figure S4 | Norepinephrine enhances the response of astrocyte processes in V1 to light stimulation, related to Figure 4. **A,** Evoked extracellular voltage change (black trace, average of 35 trials) recorded ~150 µm below the pial surface in V1 in response to light exposure for the period indicated by the blue bar. **B,** Left, in vivo fluorescence image of blood vessels filled with dextran-rhodamine labeled plasma in V1. Right, change in area of blood vessel (suprathreshold pixels within highlighted region of interest on the left) induced by light stimulation representing visually evoked hyperemia. Identical intensity and duration of light was used for both measurements and for all light evoked imaging experiments in this study. **C**, In vivo GCaMP3 fluorescence of V1 astrocytes presented in Figure 4A-C. **D**, Region of interest (ROI) map outlining all GCaMP3^{+} astrocytes in the imaging area. **E**, ROI map used to calculate fluorescence changes in astrocyte somata. **F**, ROI map used to calculate fluorescence changes in astrocytes processes (somata blanked). **G**, Plots showing the fluorescence change exhibited by astrocyte processes (black trace) to enforced locomotion alone (green vertical bar), light stimulation alone (blue vertical bar), and simultaneous enforced locomotion and visual stimulation (gray bars). Red traces represent EMG activity. Arrowheads highlight a Ca^{2+} elevation and EMG activity associated with spontaneous locomotion. **H**, Graph of the mean change in GCaMP3 fluorescence for all astrocyte processes in each condition (16 - 20 trials). Colored lines connect data points from individual mice. Asterisks indicate significant difference (one-way ANOVA with Bonferroni post-hoc test). Red circles represent the mean of all trials.

Movie S1 | Series of *in vivo* two-photon images through the cerebellar cortex of an adult *GLAST-CreER;R26-lsl-tdtomato* mouse, related to Figure 1. Left, singIe optical section. Right, white bar within side view highlights imaging depth of single optical section on left. Imaged volume was 250 µm x 250 µm x 250 µm. Step size in z-direction was 2 µm; for display purposes side view image was oversampled in z-direction 8-fold followed by interpolation.

Movie S2 | Locomotion induced Ca^{2+} elevations in cerebellar Bergmann glia, related to Figures 1 and 2. *In vivo* two-photon imaging time series. Optical section 70 µm below pial surface through the cerebellar molecular layer of an adult *GLAST-CreER;R26-lsl-GCaMP3* mouse. Imaging area: 400 µm x 400 µm. Video was accelerated 2-fold. Green bar indicates average locomotion speed during displayed image frame.

Movie S3 | Locomotion induced Ca^{2+} elevations in visual cortex astrocytes, related to Figure 3. *In vivo* two-photon imaging time series. Optical section 60 µm below pial surface through primary visual cortex (V1) of adult *GLAST-CreER;R26-lsl-GCaMP3* mouse. Imaging area: 400 µm x 400 µm. Video was accelerated 2-fold. Red bar indicates average increase in EMG activity compared to rest and green bar indicates average locomotion speed during displayed image frame.

SUPPLEMENTAL EXPERIMENTAL PROCEDURES

All procedures were approved by Johns Hopkins University Animal Care and Use Committee.

Animals. *Gene Targeting in Embryonic Stem Cells and Generation of R26-lsl-GCaMP3 Knock-In mice.* Conditional GCaMP3 mice were generated using a knock-in strategy into the ROSA26 locus. For inducible expression of GCaMP3, we incorporated a transcriptional "stop" sequence (3x SV40 polyA) flanked by loxP sites (loxP-stop-loxP, LSL); the presence of the stop sequence prevents expression of GCaMP3 until Cre recombinase excises this DNA. To have ubiquitous and robust expression, we engineered GCaMP3 under control of the CAG promoter, a chicken β-actin promoter with a 5' cytomegalovirus early enhancer element, and as a 3' UTR we incorporated WPRE (woodchuck hepatitis virus posttranscriptional regulatory element) sequence. WPRE leads to the early exit of mRNA from the nucleus as well as enhances the stability of mRNA in the cytosol. The final GCaMP3 targeting vector (pAA004) was assembled by cloning *CAG-LSL-GCaMP3-WPRE* gene fragment into a ROSA26 targeting plasmid (obtained from Dr. Jeremy Nathans at Johns Hopkins University) containing 2.2 kb 5' homology arm, 4.3 kb 3' homology arm, PGK-Neomycin resistance cassette (immediately upstream of 3' homology arm) for positive selection and PGK-DTA (downstream of 3' homology arm) for negative selection. The embryonic stem (ES) cells derived from a SV129 mouse strain were electroporated with the *AsiSI* linearized targeting vector pAA004. A nested PCR screening strategy along the 5' homology arm was used to identify ES cell clones harbouring the correct genomic targeting event. To confirm the proper targeting, southern blot analysis was performed on *EcoRI* digested genomic DNA isolated from PCR positive ES cell clones and probed with a 494 bp long P^{32}-labeled probe located 123 bp upstream 5' homology arm of ROSA26 gene. In order to confirm the integrity of targeted ROSA26 locus, *EcoRI* digested ES cell genomic DNA was probed with P^{32}-labeled 375 bp probe located 2.9 kb downstream of 3' homology arm of ROSA26. After confirmation of the karyotypes, two correctly targeted ES cell clones were used to generate chimeric mice by injection into blastocysts derived from SV129 females at the Johns Hopkins University Transgenic Core Laboratory. Germ line transmission was achieved by breeding male chimeric founders to C57Bl/6N wild-type female mice. Routine genotyping of *R26-lsl-GCaMP3* mice was performed by PCR using primers following primers: R26U1 (ROSA26-s, 5'-ctctgctgcctcctggcttct-3'), R26U2 (ROSA26-as, 5'-cgaggcggatcacaagcaata-3') and R26U3 (CMV-enhancer-as, 5' tcaatgggcgggggtcgtt-3'). These primers will amplify a 327bp DNA fragment for the wildtype ROSA26 allele, 247 and 327 bp fragments for heterozygous GCaMP3 mice, and a single 247 bp fragment for homozygous GCaMP3 mice. The presence of the Neomycin resistance cassette did not have any adverse effects on the expression of GCaMP3 or the health and survival of *R26-lsl-GCaMP3* mice. Hence, in the current study our mice still harbour the flipped PGK-Neomycin resistance gene. This cassette can be removed by crossing GCaMP3 heterozygous mice to FLP deleter mice. *GLAST-CreER;R26-lsl-GCaMP3* mice were injected with 3 x 100 mg/kg body weight of tamoxifen i.p. at 48 hour intervals at P21-P30, surgery was performed on 4-5 week old animals and imaging sessions were begun at least two weeks later. For routine imaging, 35 µl of 3% dextran-rhodamine (MW 70,000) in saline was injected into one of the saphenous veins.

Animal surgery. Craniotomies were performed in two steps. In the first surgery, a custom designed stainless steel plate was attached to the skull for immobilization of the head under the objective. In the second surgery, performed at least 3 days later, the bone was removed and replaced with a coverslip. Mice were anaesthetized by i.p. injection of ketamine (100 mg/kg) and xylazine (10 mg/kg). As soon

as animals were unconscious, petroleum jelly was applied to the eyes. The scalp was incised, resected, and a mixture of lidocaine HCl and epinephrine (Hospira; 10 mg/ml and 10µg/ml, respectively) were applied topically before the skull was exposed. For surgeries on the cerebellum, superficial neck muscles were resected to expose the skull above vermis and left hemisphere. For all surgeries, the periostium was then shaved off and approximately 3 mm of muscle surrounding the exposed skull was covered with a thin layer of cyanoacrylate cement. After drying, an 11 mm wide aluminum head plate with a 4 mm x 6 mm oval opening was centered above crus II / paramedian lobule of the cerebellar hemisphere (Figures 1, 2; Figure S2), above primary visual cortex V1 at lambda, 2.5 mm lateral from midline (Figures 3, 4; Figures S3, S4) or above transverse sinus between V1 and lobulus simplex (Figure 3F-H), and attached to the skull using dental cement (C&B Metabond; Parkell Bio-Materials Div.). The second surgery was performed at least three days (at least one week for acute imaging experiments; Figure 2G) after mounting of the head plate under ketamine / xylazine anaesthesia (under 1.5-2 % vol./vol. isoflurane in O_2 for acute imaging experiments). A 2.5 mm x 2.5 mm (2.5 mm x 5 mm for Figure 3F-H) area of skull in the center of the opening was removed using a scalpel blade #12. A No.1 cover glass was placed on the dura mater and the edges sealed with dental cement (Caulk Division, Dentsply International; Grip Cement). Imaging was initiated at least two weeks after surgery. The time during recovery from the second surgery, or between first and second surgery for acute imaging experiments, was used to habituate the mouse to the linear treadmill and the imaging environment.

***In vivo* two photon imaging.** Fluorescence images were collected using a Movable Objective Microscope (MOM) (Sutter Instrument) with a Zeiss 20x, 1.0 NA objective. The microscope was controlled by a personal computer equipped with an Intel Core i7 CPU 950 @ 3.07 GHz and 3 GB of RAM running ScanImage (v3.6) software (Pologruto et al., 2003) and custom scripts modified from TrImager software (Paukert and Bergles, 2012). Acquired frames were 400 µm by 400 µm at 512 by 512 pixel resolution. Image acquisition rate was 2 frames/s. Two photon excitation was achieved using a Titanium:Sapphire laser (Chameleon Ultra II, Coherent) tuned to 900 nm and attenuated, so that an average power of 45 mW or less entered the brain. The head of the mouse was immobilized by attaching the head plate to a custom machined stage mounted on the microscope table. Mice were kept on the stage for a maximum of two hours.

Dual optic fiber bundle imaging. For simultaneous single photon fiber optical imaging of cerebellum and visual cortex, the optical axes of the two fiber bundles at the animal's ending were arranged with a separation of 3.5 mm. The excitation light from the fiber bundles was focused into the tissue and the emitted light was collected through coupling / objective lenses placed in close proximity to the cover glass of the cranial windows (see schematic in Figure 3F). The following parts were used for the microscope: 488 nm laser, OBIS488LS 20 mW, Coherent; 10x beam expander, BE10M-A, Thorlabs; dichroic mirror, FF499-Di01-25x36, Semrock; objective lens, Plan 4x/0.10 NA Olympus; fiber bundles with 650 µm diameter - 600 µm diameter field of view, FIGH-30-650S, Fujikura; coupling/objective lens, aspheric lens pair, 352140-A/0.55NA, Thorlabs; GFP emission filter; focusing lens, achromatic doublet lens, AC254-150-ML-A, Thorlabs; CCD camera, GS2-FW-14S5M, Point Grey Research. Optical cross-talk between the fiber bundles was minimal: The coupling / objective lens pairs had a diameter of 2.4 mm and a working distance of 0.88 mm. Thus, with a distance of 3.5 mm separating the optical axes of the two fiber bundles, capturing light from the other structure would be very inefficient. If such cross-talk occurred and Ca^{2+} responses in cerebellum and visual cortex did

not co-vary, we would expect many instances of small responses in one probe accompanying robust responses in the other; however, the majority of responses were of similar size (Figure 3H). In addition, if cross-talk between fibers was the cause of co-variation, responses measured by the two fibers should have the same kinetics; however, while the onset of the two signals was not significantly different, the signal from visual cortex reached its peak significantly later than the signal from cerebellum.

Locomotion behavioral paradigm. Head immobilized mice were placed on a custom designed linear treadmill. The treadmill was either freely movable so that animals could move at will, or it was under motor control. The motion of the belt of the treadmill was monitored with a mechanically coupled optical encoder. The signal of the optical encoder was digitized at 20 kHz simultaneously with the mirror position signal of the slow scan galvanometer (Digidata 1440A, Molecular Devices) for post hoc determination of movement velocity during corresponding images.

Electromyography. Body surface potentials were recorded as the voltage difference between two silver wires placed subcutaneously at the right shoulder and left hip using an electrocardiogram amplifier (Sigmann Elektronik) and an instrumentation amplifier (Brownlee Precision; Model 440). Data were digitized at 20 kHz (Digidata 1440A, Molecular Devices) for post hoc analysis. Muscle activity was extracted by applying a fast Fourier transform to the data and determining the power in the range 200 Hz - 1 kHz. Fold increase was determined as power / $power_{Baseline}$.

Visual stimulation. A UV-LED (UVTOP-355-TO39-FW, Sensor Electronic Technology Inc.) with a Lambertian emission profile was used as a light source at a distance of 40 mm centered between the eyes to achieve uniform light exposure. The light power entering each eye with a pupil diameter of 2 mm was 7 nW. To eliminate optical cross talk between visual stimulation and two-photon fluorescence detection, the objective was shielded from the light source.

Visual evoked potential recordings. A 3 mm x 3 mm area of bone covering primary visual cortex was removed under isoflurane anaesthesia (1.5-2 % vol./vol. in O_2) from 4 week-old *GLAST-CreER;R26-lsl-GCaMP3* mice, as described above. The brain was covered with artificial cerebrospinal fluid (ACSF), containing in mM: 137 Na^+Cl^-, 2.5 K^+Cl^-, 1 $Mg^{2+}Cl^-_2$, 2 $Ca^{2+}Cl^-_2$, 20 Hepes, pH adjusted to 7.3 using NaOH. The tip of a glass micropipette filled with ACSF and a tip resistance of 6 MΩ was placed 150 µm below the pial surface. The reference electrode was placed on the surface of the bone covering the rostral forebrain and submersed in ACSF solution. The potential difference was recorded in current-clamp mode using a Multiclamp 700B amplifier (Molecular Devices) and recordings were filtered at 5 kHz and digitized at 20 kHz (Digidata 1440A, Molecular Devices). Visual stimulation episodes lasting 5 s were delivered once per minute.

Pharmacology. *Systemic:* Mice were exposed to the following dosages of solvents for i.p. injection of lipophilic drugs (µl/10g body weight): trazodone: 3 DMSO + 3 Tween 80; metergoline: 5 DMSO + 5 Tween 80; 2-Methyl-6-(phenylethynyl)pyridine (MPEP): 18 DMSO; AM251: 3 DMSO + 6 Tween 80. *Acute* (Figure 3G): In order to optimize access of drugs to the cerebellum while preserving integrity of the tissue we removed the dura following removal of the skull and continuously superfused the surface of the cerebellum with ACSF. In order to dampen tissue movement associated with the mouse walking on the treadmill we cemented (Caulk Division, Dentsply International; Grip Cement) a

3 mm (rostrocaudal direction) by 800 μm strip of No. 1 cover glass across the skull window. The center 2 mm of the glass strip was extended by gluing an additional 2 mm by 800 μm strip of No. 1 cover glass to it using a UV curable optical adhesive (Norland Optical Adhesive 61, Norland). This procedure provided sufficient gentle pressure against the surface of the cerebellum to enable two-photon imaging during locomotion events while providing access for diffusion of drugs into the underlying tissue that was imaged.

Immunocytochemistry. Mice were perfused by cardiac puncture with 4% paraformaldehyde in phosphate buffer (PB). Brains were then removed and immersed in the same fixative for 4 h at 4°C. Free-floating parasagittal sections (35 μm) were prepared using a Vibratome (VT1000S, Leica) and collected in PB. Sections were rinsed, blocked against nonspecific antibody binding, and permeabilized in PB containing 5% normal donkey serum (NDS) and 1% Triton X-100 for 3 h. Sections were then incubated for 36 h at 4°C in PB containing 5% NDS, 0.5% Triton X-100, primary antibodies, rabbit α-GFAP (1:500, Millipore) and guinea pig α-GFP (1:500, gift from M. Fukaya) (Figure 1A), and rabbit α-GFAP (1:500, Millipore) and goat α-GFP (1:200, SICGEN) (Figure 3A, B and Figure S1). After rinsing, sections were incubated for 3 h at room temperature in PB containing 5% NDS and Cy2- and Cy5-conjugated secondary antibodies against guinea pig or goat and against rabbit (1:1000; Jackson ImmunoResearch), respectively. Images in Figures 1A and 3B were obtained using a Zeiss LSM 510 confocal microscope with a Zeiss 40x oil immersion, 1.3 NA objective and the pinhole set to less than 1 airy unit. Images represent maximum intensity projections of image stacks with a step size of 0.5 μm covering 8-10 μm. Figure 1A represents a tiled image. The image in Figure 3A was taken at a Zeiss AX10 Imager M1 microscope using a Zeiss 2.5x, 0.12 NA objective.

Data Analysis. Data were processed and analyzed in MATLAB using built-in functions integrated into custom routines. Images were first processed with a Gaussian filter (1.52 SD per pixel distance) to reduce stochastic noise of the detector. To compensate for motion artifacts during image series, a whole-frame normalized 2D cross-correlation (built-in function “normxcorr2”) was determined for dextran-rhodamine images, and individual frames were registered to maximize correlation. The same registration parameters were then applied to images of GCaMP3 fluorescence. ΔF/F fluorescence intensity ("Ca^{2+} change") traces represent $(F - F_{median}) / F_{median}$ with F representing mean fluorescence value of all pixels within a region of interest (ROI) of one image frame and F_{median} representing median F of all image frames. ROIs were the entire image frame (Figures 1, 2 and Figure S2), thresholded area distinguishing GCaMP3 expressing astrocytes from background (Figures 3C-E, 4A and D, Figure S3), individual astrocytes (Figure 4A-C) or area representing each fiber bundle (Figure 3F-H). Quantification of individual Ca^{2+} responses represents the peak (Figures 1E, 3H) or mean ΔF/F within 0 -10 s (cerebellum) or 2.5 - 12.5 s (visual cortex) following the onset of locomotion or stimulation. For the analysis of astrocyte responses to light stimulation alone in Figure 4D, we analyzed trials in which during the episode from 2 s preceding light stimulation until 2 s following light stimulation the EMG signal never exceeded 2.2 fold relative to baseline. This criterion was chosen to exclude trials during which the mouse voluntarily engaged in locomotion or showed a startle response. For analysis of the correlation between the magnitude of the Bergmann glia Ca^{2+} change and locomotion speed (Figure 1E), we used the following statistical strategy to identify response failures to locomotion (which were excluded from the correlation analysis): we determined the mean and standard deviation (SD) of 15 consecutive ΔF/F values preceding the onset of locomotion (baseline). If the difference between the mean of the 10 largest ΔF/F values within 15 consecutive ΔF/F values from onset of

locomotion and the mean of the baseline did not exceed 2 * SD of the baseline, it was considered a failure.

Statistical Analysis. Figures 1E and 3H: analysis of co-variance for correlation within subjects (Bland and Altman, 1995); Figures 1B and C, 4D (right), difference in onset of response in Figure 3F-H, Figures S2 and S3, one-tailed paired *t* test; Figures 1F and G, 4C and D (left) one-way ANOVA followed by Bonferroni post-hoc test; text, difference in peak of response in Figure 3F-H, one-sample *t* test.

References

Bland, J.M. and Altman, D.G. (1995). Calculating correlation coefficients with repeated observations: Part 1 - correlation within subjects. BMJ *310*, 446.

Paukert, M. and Bergles, D.E. (2012). Reduction of motion artifacts during in vivo two-photon imaging of brain through heartbeat triggered scanning. J. Physiol. *590*, 2955-2963.

Pologruto, T.A., Sabatini, B.L., and Svoboda, K. (2003). ScanImage: flexible software for operating laser scanning microscopes. Biomed. Eng. Online *2*, 13.